Investigations of interfacial waves at the inlet section in stratified oil–water flows

A.H. Barral, A. Ebenezer, P. Angeli *

Department of Chemical Engineering, University College London, London, UK

ABSTRACT

The formation and evolution of oil–water interfacial waves at the inlet section of a horizontal test pipe was investigated experimentally via high-speed imaging. Images were collected with a Phantom Miro 4 high-speed camera at a rate of 1000 fps. Wave velocity, amplitude, frequency and wave length at different oil–water flow rates (input ratios, $r = 0.6$–2.5; mixture velocities, $U_{mix} = 0.8$–2 m s^{-1}) were calculated from the images. The fluids used were tap water ($\rho = 1000$ kg m^{-3}, $\mu = 0.001$ kg m^{-1} s^{-1}) and Exxsol D140 oil ($\rho = 830$ kg m^{-3}, $\mu = 0.0055$ kg m^{-1} s^{-1}). The waves formed via a KH mechanism immediately after the junction where the two fluids joined and at a velocity roughly equal to half the mixture velocity with a frequency in the range 11–20 Hz for all flowrate combinations. Once formed, and at a short distance from the junction the wave amplitudes decreased while the wave velocities and the wavelengths increased. The frequency, however, remained constant. Experimental data was compared against predictions of the wave theory and the instability analysis. The propagation of interfacial waves at half the mixture velocity was predicted by the theory of dynamic waves. Results from the inviscid stability analysis at the inlet agreed qualitatively with the flow pattern map observed well further downstream the inlet, but quantitative differences were seen, which could be due to the viscosity of the oil phase.

© 2014 The Authors. Published by Elsevier Inc. This is an open access article under the CC BY license (http://creativecommons.org/licenses/by/3.0/).

1. Introduction and background

There have been many research efforts in recent decades directed towards understanding and predicting the flow behaviour of oil–water mixtures in pipes. A particular area of interest is the identification of the flow patterns that establish under different conditions and their effect on pressure drop and heat and mass transfer rates. Different patterns and their boundaries were studied by a number of investigators (see the review of Trallero [1] until 1995 and later on e.g. Valle and Utvik [2]; Lovick and Angeli [3]; and Chakrabarti et al. [4]). An important flow pattern transition is from separated to dual continuous flows, where both phases are continuous and drops of one phase appear in the other phase. This transition has been generally related to the appearance and growth of waves on the oil–water interface and the detachment of drops from them (see, for example: Ishii and Grolmes [5] in gas–liquid; Brauner and Moalem Maron [6] and Kadri et al. [7] in liquid–liquid). Different wave types have been identified in gas–liquid flows (Andritsos and Hanratty [8]); visualisation techniques are often used for their study, particularly when the waves appear as large, almost two dimensional and readily identifiable structures (Andritsos [9]; Ng et al. [10]).

The types of interfacial waves seen in oil–water flows depend on the fluid properties. With high viscosity oils, two dimensional structures tend to form, which can be studied with visual techniques. With the aim of improving lift–off for heavy oil recovery, Oliemans et al. [11] investigated interfacial waves in annular flow. Rodriguez and Bannwart [12] also studied annular flows in vertical pipes, and measured wave characteristics using image analysis. Recently, other parameters of the flow (e.g. water fraction) were determined from image analysis in systems involving heavy oils (Riano et al. [13]). Stratified flows with low viscosity oils, however, can exhibit fluctuating interfaces where visual analysis can be challenging because of the lack of easily identifiable wave structures. Although Al-Wahaibi and Angeli [14] were able to investigate interface development in separated flows with a low viscosity oil using high-speed imaging, De Castro et al. [15] applied a filtering technique to overcome the difficulties in image analysis with fluctuating interfaces. In this way, they calculated wavelengths, amplitudes, velocities and the shape of the resulting waves after the image filtering. Barral and Angeli [16] used a conductance probe to study the fluctuating oil–water interface in fully developed flow. By applying a spectral density analysis to the time series signal of the probe they were able to identify the contributing

---

Nomenclature

C_v	wave velocity
f	frequency
$f_{\nabla\alpha}$	stabilizing fore
KH	Kelvin–Helmholtz
r	oil-to-water input ratio
t	time
u_o	actual velocity of oil phase
u_w	actual velocity of water phase
U_{mix}	mixture velocity

U	weighted average velocity
W_u	weighted mean velocity
Greek symbols	
α	water fraction
μ_o, μ_w	viscosity of oil, water
ρ_o, ρ_w	density of oil, water
σ	oil–water interfacial tension

---

frequencies of the interface. Interestingly, they found that the large, almost two dimensional waves forming at the inlet of the test section had a characteristic weighted frequency of 19 Hz, which was preserved further downstream despite the fact that large waves gave place to smaller three-dimensional structures.

In this work, the large, almost two-dimensional oil–water interfacial waves that form at the inlet section of a horizontal test pipe when the oil-to-water flowrate ratios are different from 1 are investigated. These waves form immediately after the two phases join and reduce in size in a very short distance downstream, where they are replaced by small three dimensional structures that characterise the oil–water interface further downstream the horizontal pipe. This is contrary to the common expectation that waves grow along the pipe and may result in a flow pattern transition. The clear 2D wave structures of the inlet waves make possible their investigations by means of high-speed imaging. The nature of interfacial waves at the inlet is studied and an explanation for their dampening further downstream is presented.

2. Experimental set-up and data acquisition

Experiments were performed in the oil–water flow facility of the Multiphase Flow Lab in the Department of Chemical Engineering, UCL. The rig consists of a 38 mm ID horizontal acrylic test section, which allows the visual inspection of the flow. The test fluids used are tap water (ρ = 1000 kg m^{-3} and μ = 0.001 kg m^{-1} s^{-1}) and Exxsol D140 oil (ρ = 830 kg m^{-3} and μ = 0.0055 kg m^{-1} s^{-1}), where ρ and μ are density and viscosity, respectively. The two fluids are stored and pumped separately using centrifugal pumps. Their flow rates are regulated (variable from 20 L min^{-1} up to 250 L min^{-1}) via control valves and measured separately with variable area flow metres (ABB Instrumentation Ltd.) with accuracy of 1% full scale. Fig. 1 shows a schematic of the experimental facility while the inlet section and its location in the facility is shown in Fig. 2 in more detail.

The inlet section is made within an acrylic block and has an asymmetric Y-shape, with the upper duct (inlet for oil) inclined 10° downwards and the lower one horizontal (inlet for water), both with 38 mm ID (Fig. 2a). The fluids join smoothly at the junction point of the two ducts without the use of a split plate. A split plate is sometimes used to enhance stratification and delay transition to dual continuous flow, but it was found in this work to have the opposite effect, i.e. it increased mixing and promoted drop formation. High-speed images have been collected at about 8–12 cm after the junction point of the phases, which is the distance needed by the waves to form, towards the end section of the inlet over a length of about 16 cm (Fig. 2a). Waves formed immediately after the two phases joined at the junction and were seen to dampen quickly downstream, within the inlet section.

After the test section which has an overall length of about 16 m, the mixture of the two fluids is returned into a separator vessel equipped with a Knit Mesh™ coalescer. Oil and water are then

returned from the top and the bottom of the separator respectively into their storage tanks.

The interfacial waves that developed at the inlet were investigated for more than 20 oil–water flowrate combinations, with oil-to-water flowrate ratios, r, varying between 0.6 and 2.5 and mixture velocities, U_{mix}, varying between 0.8 and 2 m s^{-1}. As two dimensional, visually-identifiable waves did not develop at the inlet for r = 1, only flowrate ratios different than 1 were studied. Fig. 3a and b show two snapshots of typical waves at the inlet, for input flowrate ratios lower and higher than 1, respectively. A high speed video camera (Phantom Miro 4) was used to investigate such waves and to record the flow pattern. Images were taken at 1000 frames per second (fps). Up to 4200 frames could be stored in the camera memory, giving a recording time of 4.2 s. This time span was found to be sufficient to capture the evolution of a large number of waves (i.e. interface developments were typically in the time scale of a few milliseconds). In many cases, for practical purposes, a smaller time interval was selected, which allowed 20–25 waves to be captured and analysed for each oil–water flow rate.

The interfacial wave characteristics were acquired from the images taken using a pre-calibrated scale. Fig. 4 shows a typical high-speed image and the reference lines used for analysis. Each image was divided in 4 regions and fixed locations were taken within each region at more or less equal distances (Fig. 4 shows actual distances in cm). Waves were then identified and followed as they moved across the fixed locations of the regions. As mentioned, high-speed images were taken a few centimetres after the junction point where the phases joined. The overall distance required by the waves to form after the junction was found to be about 8–12 cm (2–3 times the pipe diameter), which was independent of the flow conditions (i.e. input ratio and mixture velocity). Therefore, the formation of waves was observed to be faster for faster flows. As example, for a flow with U_{mix} = 0.85 m s^{-1} (shown in Fig. 4) waves formed in about 0.24 s, which is the time required to travel a distance of 10 cm (as will be discussed later, developing waves travel at roughly half the mixture velocity).

To calculate the average interface height, the height of the interface from the bottom of the pipe was recorded in each image at 25 locations equally spaced; the spatial resolution was therefore approximately 0.64 cm (i.e. one measurement every 0.64 cm along the inlet at each time instant). In order to obtain distinct measurements at each location, images separated by 5 ms were analysed. The images collected at 1000 fps could be clearly resolved at this level, which seems to be in agreement with the sampling frequency of 256 Hz used by Barral and Angeli [16] to satisfy the Shannon Theorem. A total of 38 images were collected for each set of flowrates, over a period of 190 ms, which gave 38 values at each location within the inlet for the calculation of the average interface height. Fig. 5 shows, as example, the development of the average interface height along the inlet at input ratio, r = 2.5, and mixture velocity, U_{mix} = 1.03 m s^{-1}. Average interface height measurements were
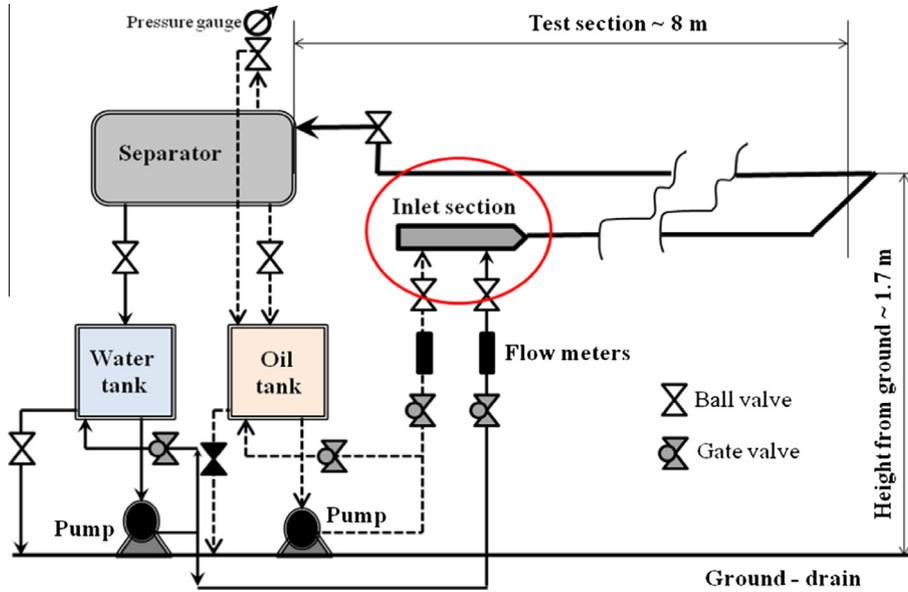
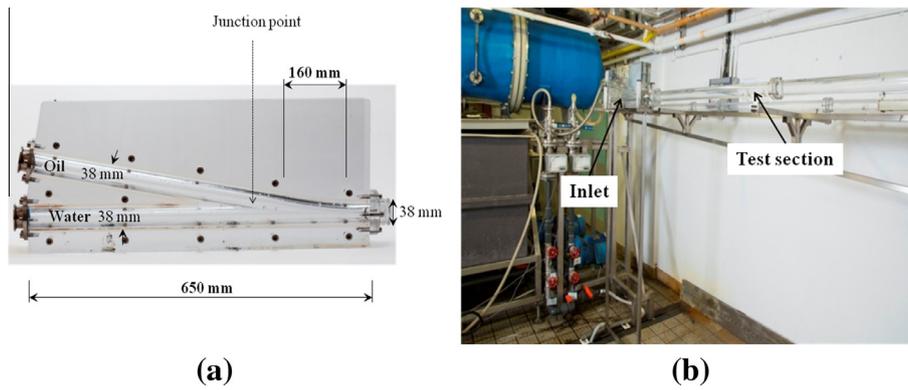Fig. 1. Schematic of the experimental facility.

Fig. 2. Inlet section of the oil–water flow facility. (a) Inlet section. Junction point is where the two phases join. Images were collected over the 160 mm distance shown. (b) Location of the inlet section in the flow facility.
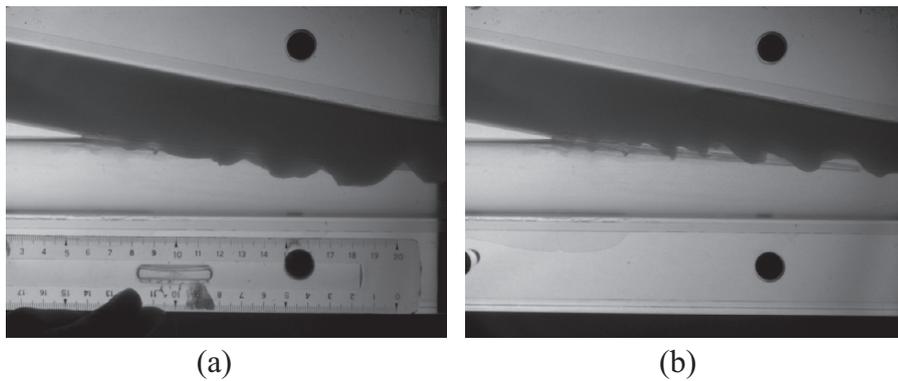

Fig. 3. Formation of waves at the oil–water interface in the test section inlet for input oil-to-water flowrate ratios different from 1. (a) $r = 2.6$; $U_{mix} = 1.13$ m s^{-1}, (b) $r = 0.61$; $U_{mix} = 1.21$ m s^{-1}.

performed for all the oil–water flowrate combinations used in this work. It was found that the average interface height typically decreased along the inlet for all conditions studied.

Since the waves observed did not have perfect sinusoidal shapes, the wave crests were used to calculate the wave ampli-

tudes. In these measurements, the height of each crest that passed from each fixed location in the four regions (see Fig. 4) was measured from the bottom of the pipe. The amplitude of the wave at each fixed location was then found by subtracting the average interface height from the crest height. Amplitudes were measured
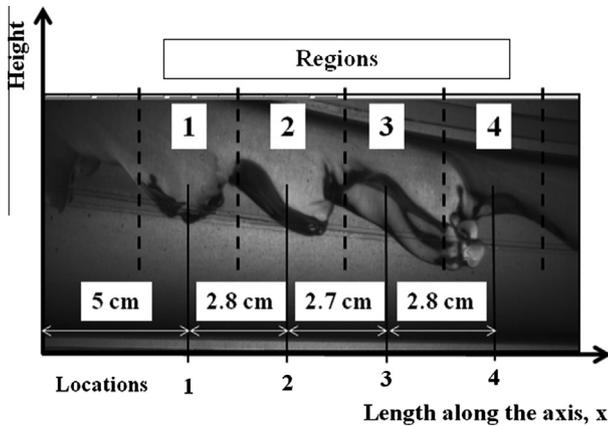
Fig. 4. Image of the waves at the inlet section ($r = 0.6$; $U_{mix} = 0.85$ m s^{-1}) over the 160 mm distance shown in Fig. 2a. The regions used for analysis (actual distances) are shown.
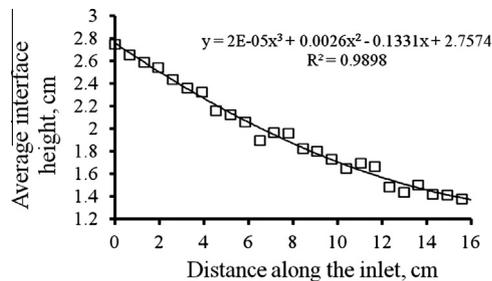

Fig. 5. Average interface height along the inlet section ($r = 2.5$ and $U_{mix} = 1.03$ m s^{-1}) and fitted line.

on a minimum of 20 waves in all cases (typically, between 20 and 25).

Velocities were calculated from the time taken by a given wave crest to move from a fixed location in one region to another fixed location in the next region and the distance between the two locations. Three values were therefore computed along the inlet (i.e. between regions 1–2, 2–3 and 3–4). The frequency of the waves was taken as the inverse of the time interval between two crests at each fixed location and, thus, the frequencies could be measured four times along the inlet (i.e. at locations 1, 2, 3 and 4). The wavelengths between regions were calculated from the wave velocities and the frequencies. Again, wave velocities and wavelengths have been obtained for a minimum of 20 waves in all cases.

The relative uncertainty in measuring distances on the image depends on the value of the distance measured, but the average error between the fixed locations in the 4 regions can be estimated as no more than 4%, with an uncertainty of the measurement from the left side of the image of ±0.2 cm. The uncertainty in velocities and wavelengths tends to decrease towards the end of the inlet, because both increase in value. To calculate an average uncertainty it is assumed that the error of time variable is negligible (at least compared to that of measurements on the image), and about 6.5% error in velocity and 8% in wavelength were found. The uncertainty of the amplitude increases along the inlet, because the amplitude of the waves decreases. The estimated error in measurements of amplitude is no more than 10% in all cases. This figure comes from the propagation of errors in measuring the height of the crests (about 3.5% at $r > 1$ and 1% at $r < 1$), the average height of the interface (about 6.5% at $r > 1$ and 4% at $r < 1$) and the uncertainty of the regression line of the average interface height (see Fig. 5), which has an average of ∼5%.

3. Results

Interfacial waves were studied after the junction point at the inlet for oil and water flowrate combinations which gave stratified flow downstream the pipe. As it has been noted, it was found that waves formed at the inlet when the input flowrate ratio was different than 1, while no waves formed when the flowrates were similar.

The evolution of the average interface height along the inlet section as a function of the oil-to-water ratio, r, is summarised in Figs. 6 and 7. To enable comparisons across different flow rates, the interface heights shown in Fig. 6 are non-dimensionalised by dividing the measured interface heights over the maximum value, found at the left side of the image (i.e. $x = 0$ in Fig. 4). The actual interface height can be seen in Fig. 7, where it is plotted against the input ratio r. It was found that in all cases, the interface height decreases along the inlet. This trend reflects the geometry of the inlet where the top duct (i.e. oil inlet) still has a negative slope for a few centimetres after the junction point (Fig. 2a). However, as can be seen in Fig. 6, the decrease in interface height is larger for $r = 2$, where the oil flowrate is higher than that of water, compared to $r = 0.5$. This suggests that the interface adjusts faster in this case within the same distance.

Both Figs. 6 and 7 show that the average interface height depends mainly on the input ratio and it is not affected by the mixture velocity. This has been verified against experimental data collected at different oil-to-water flowrates, with an example shown in Fig. 8 for $r = 2.2$. As can be seen, the average interface height is independent of the mixture velocity.

Despite the fact that these experimental results are concerned with the formation and evolution of waves at the inlet section, it is worth to note that similar conclusions on the effects of input ratio and mixture velocity on interface height have been reached by other researchers investigating stratified flows in pipes at distances further downstream the inlet (Kumara et al. [17]; Barral and Angeli [18]).

The visual observations at the inlet showed that waves form when the two fluids join but quickly decrease in size within the inlet section until they eventually disappear. Fig. 9 shows the wave amplitudes from zones 2 to 4 relative to the amplitudes of the waves in zone 1. Relative average values and standard deviations are $0.85 \pm 10.7\%$ in region 2, $0.707 \pm 15.1\%$ in region 3 and $0.562 \pm 19.0\%$ in region 4; the standard deviation of average measurements increases as the wave amplitudes reduce. In contrast, wavelengths increased along the inlet as can be seen in Fig. 10 where the wavelengths have been normalised against the values in regions 1–2. The average values and standard deviations are $1.09 \pm 5.4\%$ across regions 2–3 and $1.20 \pm 6.5\%$ across regions 3–4.

The volume of the waves along the inlet has been estimated using the average normalised amplitudes and wavelengths at each
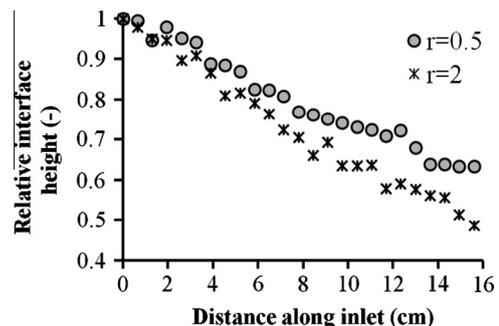

Fig. 6. Development of relative average interface height along the inlet for two input ratios different from one ($r = 0.5$ at $U_{mix} = 1.3$ m s^{-1} and $r = 2$ at $U_{mix} = 0.9$ m s^{-1}).
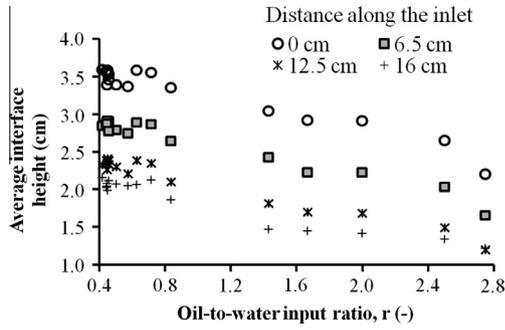
Fig. 7. Average interface height against input ratio *r* at different distances along the inlet for all mixture velocities studied.
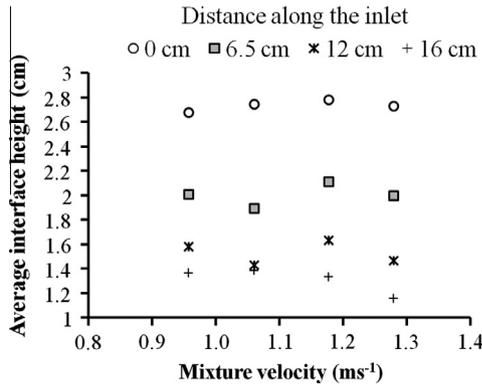

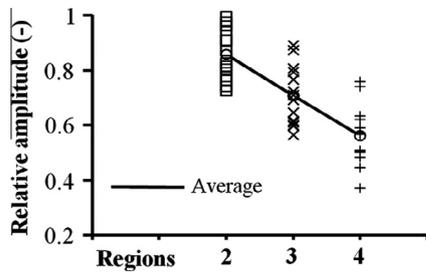**Fig. 8.** Average interface height along the inlet against mixture velocity at *r* = 2.2.

Fig. 9. Evolution of relative wave amplitudes along the inlet (*r* = 0.6–2.5; U_{mix} = 0.8–2 m s^{-1}).

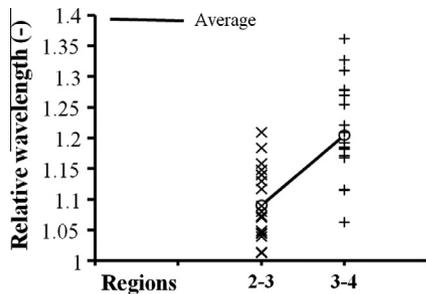**Fig. 10.** Evolution of relative wavelengths along the inlet (*r* = 0.6–2.5; U_{mix} = 0.8–2 m s^{-1}).

flowrate combination. In general, the wave volume decreases as waves move downstream, but no trend has been found with respect to the input ratio or mixture velocity.

Interestingly, for all flowrate combinations tested, wave frequencies were found to be within the range of 11–20 Hz. As can be seen in Fig. 11 the frequencies remained constant along the inlet, despite the changes in amplitude and wavelength noted.

While the wave frequencies did not change significantly, the wave velocities increased along the inlet. This result is somehow expected, since the frequencies appear to be constant while the wavelengths increase (Fig. 10).

The absolute wave velocities measured across the regions 1–2, 2–3 and 3–4 were normalised against their respective mixture velocities (Fig. 12). The region 1–2 of the images is the area closest to the point of maximum growth of the waves in the inlet and, therefore, waves at this region have maximum amplitude. The wave velocities in this region also had their minimum values in all cases. As the waves travel from region 1 in the inlet to the other regions, their amplitudes decrease while their velocities increase. The wave velocity seems to increase almost linearly with the mixture velocity as can be seen in Fig. 13. Both Figs. 12 and 13 show that the wave velocities are independent of the input oil-to-water flowrate ratio.

4. Stability analysis and nature of inlet waves

The experimental results reveal that interfacial waves develop at the inlet for input ratios different from 1 as soon as the two phases join but eventually they disappear. In addition, their frequencies are independent of the flowrates of the two fluids and remain constant. This is in agreement with results obtained from the spectral analysis of the interface signal, collected with conductance probes (Barral and Angeli [16]). Constant frequency implies constant wave period, which may suggest that the formation and, particularly, the dampening of the waves take place with very little energy dissipation (see, for example, Craik [19]).

At input ratios different from 1, oil and water phases flow with different velocities one on top of the other as they join. This is a classic case of Kelvin–Helmholtz (KH) instability, which leads to the development of waves. At input ratios close to 1 phase velocities are equal at the junction, which would eliminate the instability and support the experimental observation that no waves develop at the inlet unless the input ratio is different from 1. The stability condition of the flow at the junction point can be written as (Drazin and Reid [20]):

$$(u_w - u_o)^2 < 2\frac{\rho_o + \rho_w}{\rho_o \rho_w}\sqrt{g\sigma(\rho_w - \rho_o)}, \tag{1}$$

where u_w and u_o are the average water and oil phase velocities respectively (equal to superficial velocities at the junction), ρ_w and ρ_o are the water and oil densities respectively and σ is the interfacial tension. Eq. (1) is the classic solution of the inviscid problem, which neglects the shear stresses. This approach can be considered an appropriate approximation for the current data since the viscosity of the oil is low. Substituting the properties of the fluids used in the current work into Eq. (1) (ρ_w = 1000 kg m^{-3}, ρ_o = 830 kg m^{-3}, σ = 0.039 N m), the theory predicts that disturbances will be dampened if $(u_w{-}u_o)^2$ < 0.0357 m s^{-1}. Expanding the bracket and dividing by the squared water velocity, u_w^2, the stability condition becomes:

$$1 - 2r + r^2 < \frac{0.0357}{u_w^2} \tag{2}$$

According to Eq. (2), the oil-to-water input ratio, *r*, determines whether the wave is stable or not, but the limit of stability depends on the phase velocity (i.e. water) and, in turn, on the mixture velocity. The theory predicts that as the input ratio approaches 1 (both from *r* < 1 or *r* > 1), the stability of the flow increases and that the case *r* = 1 is the limit of complete stability.
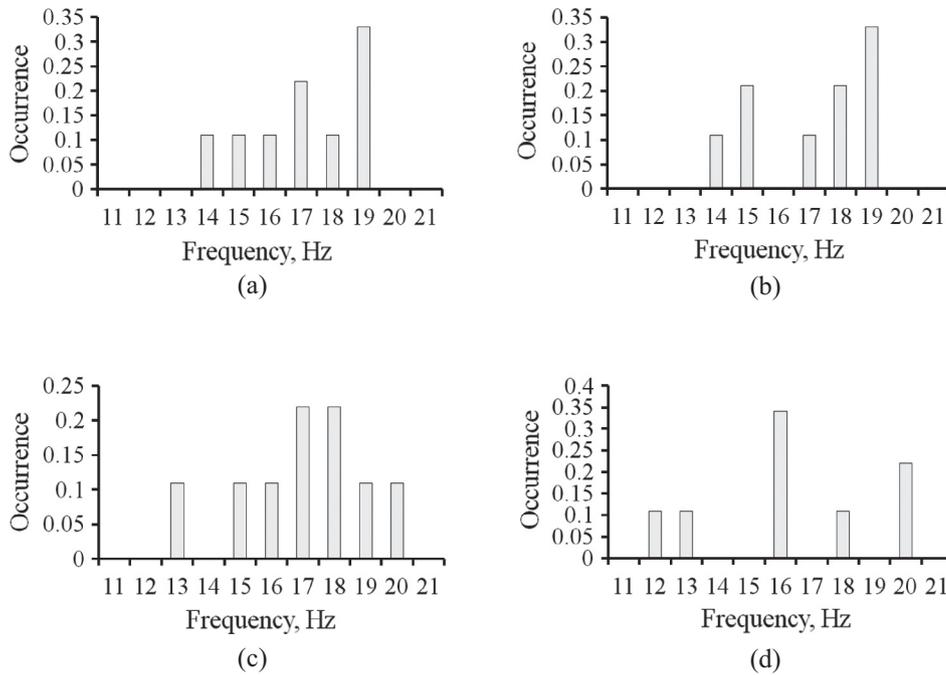
Fig. 11. Wave frequency distributions in the different regions of the inlet for $r = 1.6$ and $U_{mix} = 1.18$ m s^{-1}. (a) Region 1, (b) Region 2, (c) Region 3 and (d) Region 4.
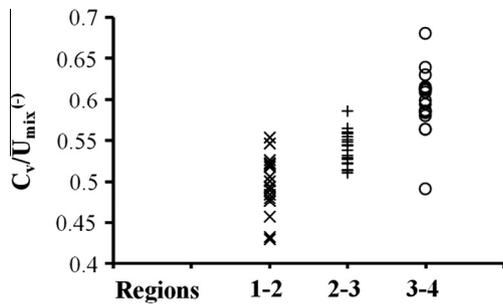

Fig. 12. Normalised wave velocity against mixture velocity at the three regions along the inlet for all conditions tested ($r = 0.4$–2.75).
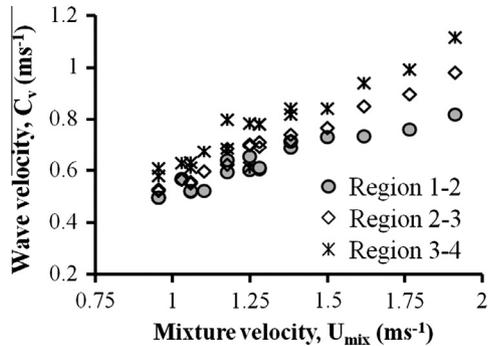

Fig. 13. Wave velocity against mixture velocity in the inlet for all input flowrate ratios tested ($r = 0.4$–2.75).

By applying Eq. (2) with some of the input ratios used experimentally, the following stability pair values were found (r; U_{mix}): (0.6; 0.823 m s^{-1}), (0.7; 1.125 m s^{-1}), (0.8; 1.588 m s^{-1}), (1.2; 1.941 m s^{-1}), (1.3; 1.522 m s^{-1}), (1.4; 1.235 m s^{-1}), (1.5; 1.103 m s^{-1}), and (1.6, 0.956 m s^{-1}). Using these points, a stability line has been plotted in Fig. 14 against the flow pattern map observed in the experimental flow facility at about 7 m downstream the inlet where the flow is considered fully developed
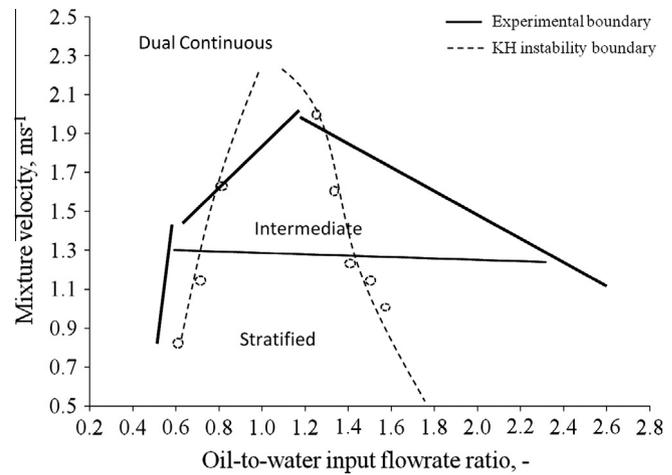

Fig. 14. Experimental flow pattern map downstream the test section (Barral and Angeli [18]) and stability line based on inlet conditions.

(Barral and Angeli [18]). In the map, the dual continuous region defines a stratified flow of oil and water completely separated by an interface with drops of one phase entrained in the other. The intermediate pattern appears between the stratified and dual continuous regimes especially at input ratios around 1 and at higher mixture velocities, and is characterised by two continuous layers, oil and water, separated by a rough interface and by very few and small sporadic drops entrained in them.

At oil-to-water input ratios, $r < 1$, the agreement between the observed map and the stability line is good, but the region of stratification is underestimated by the stability analysis at $r > 1$. At these conditions where the more viscous oil occupies a larger part of the pipe cross sectional area it is possible that viscous effects, which are ignored in the inviscid analysis, become important. Discrepancies between the stability theory and experimentation have already been pointed out by Al-Wahaibi and Angeli [21,22].

It should be noted here that the stability analysis is carried out at the inlet while the flow pattern map was obtained well

downstream of inlet. However, the comparison is still relevant since it has been observed that the final flow pattern tends to develop at the inlet and little change is seen further downstream the pipe. In particular, the drops that signify the transition from stratified to dual continuous flow were seen to form at the inlet for input ratios different from one, where waves form, while hardly any new drops were seen to form further downstream. In addition, dual continuous flow is delayed to high mixture velocities at $r = 1$, when no waves appeared at the inlet. It is reasonable, therefore, to relate the formation of drops at the inlet to the waves seen, but this needs to be verified with further investigations.

As shown in the previous section, relative amplitudes (Fig. 9) are always at a maximum at region 1 of the inlet (see Fig. 4) regardless of the mixture velocity. This finding suggests that waves develop faster in faster flows and that the increase in wave amplitude depends on the mixture velocity. This result seems to agree with the theoretical predictions of Brauner and Moalem Maron [6] for oil–water flows. Their analysis revealed that stratified flows were unstable if the imaginary part of the complex wave velocity, C_i, is positive. In this case, the wave amplification factor with respect to the top fluid (i.e. oil), C_i/u_o, increases with the velocity of the water phase, u_w. Eventually, however, waves dampen within the inlet. Studies of the fully developed flow revealed that the slip velocity between the two phases can be very small in horizontal pipes with low viscosity oils (Kumara et al. [17]; Barral and Angeli [18]). It can be argued, then, that the waves at the inlet vanish as the velocities of the phases become similar and the instability disappears.

The finding that waves at the inlet propagate at a velocity half of the mixture velocity was found to be in agreement with the predictions of the theory for dynamic waves. When considering the two main types of waves, dynamic and kinematic (or continuity), some investigators have pointed out that the stability of the flow can be entirely determined by the balance between these two types of waves; when kinematic waves overcome dynamic ones, the flow is unstable (Wallis [23]; referenced by Trallero [1]). This implies that dynamic waves are essentially a stabilizing factor to the flow. The velocity of a dynamic wave is given by (Wallis [23]):

$$C_v = \frac{\frac{\rho_o u_o}{1-\alpha} + \frac{\rho_w u_w}{\alpha}}{\frac{\rho_o}{1-\alpha} + \frac{\rho_w}{\alpha}} \pm \frac{1}{\frac{\rho_o}{1-\alpha} + \frac{\rho_w}{\alpha}} \left[\frac{-\rho_o \rho_w (u_o - u_w)^2}{\alpha(1-\alpha)} - \left(\frac{\rho_o}{1-\alpha} + \frac{\rho_w}{\alpha} \right) f_{\nabla\alpha} \right]^{0.5}, \tag{3}$$

where $f_{\nabla\alpha}$ is a stabilizing factor including viscous and body forces and α is the fraction of the pipe occupied by water. Eq. (3) can be re-arranged in terms of the mixture velocity and the oil-to-water input flowrate ratio to give:

$$C_v = \frac{U_{mix}}{r+1} \left[\frac{r\alpha\rho_o + (1-\alpha)\rho_w}{\alpha\rho_o + (1-\alpha)\rho_w} \right] \pm \frac{\alpha(1-\alpha)}{\alpha\rho_o + (1-\alpha)\rho_w}$$
$$\times \left[\frac{-\rho_o \rho_w U_{mix}^2 \left(\frac{r-1}{r+1} \right)^2}{\alpha(1-\alpha)} - \left(\frac{\alpha\rho_o + (1-\alpha)\rho_w}{\alpha(1-\alpha)} \right) f_{\nabla\alpha} \right]^{0.5} \tag{4}$$

Eq. (4) consists of two parts. The first one (before the ± sign) is called the weighted mean velocity, W_u. The second part includes the effect of a de-stabilizing factor, which is only different from 0 if r is different from 1, and of a stabilizing factor, $f_{\nabla\alpha}$. Since the two phases join in the middle of the pipe, the KH wave develops from a starting point $\alpha = 0.5$. Substitution gives the theoretical velocity of the wave at the junction:

$$C_v = \frac{U_{mix}}{r+1} \left[\frac{r\rho_o + \rho_w}{\rho_o + \rho_w} \right] \pm \frac{1}{\rho_o + \rho_w} \left[-\rho_o \rho_w U_{mix}^2 \left(\frac{r-1}{r+1} \right)^2 - \left(\frac{\rho_o + \rho_w}{2} \right) f_{\nabla\alpha} \right]^{0.5} \tag{5}$$
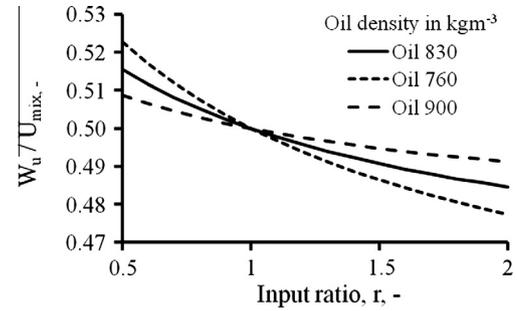

Fig. 15. Ratio of weighted mean velocity over mixture velocity against input ratio for different oil densities.

Eq. (5) shows that the dynamic wave propagates with velocity relative to the weighted mean velocity. In the limit of equal phase densities, the weighted mean velocity of the fluid becomes half the mixture velocity. For different densities (i.e. 830 kg m^{-3} oil and 1000 kg m^{-3} water), the weighted mean velocity is expected to change slightly with the input ratio, but values are around half the mixture velocity (Fig. 15).

Experimentally it was also found that the wave velocity is about half the mixture velocity in region 1 of the inlet as soon as the waves form. It can therefore be assumed that the waves developing at the inlet are dynamic; it can be argued that kinematic waves might not develop because the two liquids are incompressible and the flowrates are maintained constant. The theory cannot explain, though, the acceleration of the waves once they start reducing in size.

5. Conclusions

The formation and propagation of interfacial waves in stratified oil–water flows close to the inlet of a horizontal test section was studied with high speed imaging. It was found that waves develop very close to the inlet junction where the two fluid join (along a distance of about 8–10 cm) at velocity roughly equal to half the mixture velocity, which is in agreement with the theory of dynamic waves. After an initial increase, the amplitudes were found to decrease and the waves were dampened. This reduction in amplitude was accompanied by an increase in wavelength and wave velocity. The wave frequencies, however, did not change considerably along the inlet and were within the range of 11–20 Hz, which agrees with the frequencies found previously from the spectral analysis of the interface height variation with time obtained with a conductance probe.

Interfacial waves formed when the flowrates of the two phases were different, which suggests that the waves are created by KH instability. Drop formation and transition to dual continuous flow seems to be related to the presence of waves in the inlet and the instability. By applying the stability analysis it was possible to predict reasonably well the transition from the stratified to the dual continuous pattern observed in fully developed flow further downstream the test section for input ratios $r < 1$, but deviations were found at $r > 1$, where viscous effects might play a more significant role.

References

[1] J.L. Trallero, Oil–Water flow patterns in horizontal pipes. PhD Dissertation, University of Tulsa, 1995.

[2] A. Valle, O.H. Utvik, Pressure drop, flow pattern and slip for two phase crude oil/water flow: experiments and model predictions, in: Proc Int Symp. on Liquid–Liquid Two Phase Flow and Transport Phenomena, Antalya, Turkey, 3–7 November, 1997, pp. 63–74.

[3] J. Lovick, P. Angeli, Experimental studies on the dual continuous flow pattern in oil–water flows, Int. J. Multiphase Flow 30 (2004) 139–157.

[4] D.P. Chakrabarti, G. Das, P.K. Das, Identification of stratified liquid–liquid flow through horizontal pipes by a non-intrusive optical probe, Chem. Eng. Sci. 62 (7) (2007) 1861–1876.

[5] M.G. Ishii, M. Grolmes, Inception criteria for droplet entrainment in two-phase concurrent film flow, AICHE J. 21 (1975) 308–318.

[6] N. Brauner, D. Moalem Maron, Stability analysis of stratified liquid–liquid flow, Int. J. Multiphase Flow 18 (1) (1992) 103–121.

[7] U. Kadri, R.F. Mudde, R.V.A. Oliemans, M. Bonizzi, P. Andreussi, Prediction of the transition from stratified to slug flow or roll-waves in gas–liquid horizontal pipes, Int. J. Multiphase Flow 35 (11) (2009) 1001–1010.

[8] N. Andritsos, T.J. Hanratty, Interfacial instabilities for horizontal gas–liquid flows in pipelines, Int. J. Multiphase Flow 13 (1987) 583–603.

[9] N. Andritsos, Statistical analysis of waves in horizontal stratified gas–liquid flow, Int. J. Multiphase Flow 18 (1992) 465–473.

[10] T.Z. Ng, C.J. Lawrence, G.F. Hewitt, Evolution of interfacial structures in wavy stratified two-phase pipe flow, in: Proc 5th int conf multiphase flow, Yokohama, Japan, 31 May–3 June, 2004.

[11] R.V.A. Oliemans, G. Ooms, H.L. Wu, A. Duijvestijn, Core-annular oil/water flow: the turbulent-lubricating film model and measurements in a 5 cm pipe loop, Int. J. Multiphase Flow 13 (1) (1987) 23–31.

[12] O.M.H. Rodriguez, A.C. Bannwart, Experimental study on interfacial waves in vertical core flow, J. Petrol. Sci. Eng. 54 (3–4) (2006) 140–148.

[13] A.B. Riano, A.C. Bannwart, O.M.H. Rodriguez, Hold-up estimation in core flow using image processing, IEEE Int. Instrument. Measurement Technol. Conf. (2013) 334–338.

[14] T. Al-Wahaibi, P. Angeli, Experimental study on interfacial waves in stratified horizontal oil–water flow, Int. J. Multiphase Flow 37 (8) (2011) 930–940.

[15] M.S. De Castro, C.C. Pereira, J.N. Dos Santos, O.M.H. Rodriguez, Geometrical and kinematic properties of interfacial waves in stratified oil–water flow in inclined pipe, Exp. Therm. Fluid Sci. 37 (2012) 171–178.

[16] A.H. Barral, P. Angeli, Spectral density analysis of the interface in stratified oil–water flows, Int. J. Multiphase Flow 65 (2014) 117–126.

[17] W.A.S. Kumara, B.M. Halvorsen, M.C. Melaaen, Single-beam gamma densitometry measurements of oil–water flow in horizontal and slightly-inclined pipes, Int. J. Multiphase Flow 36 (2010) 467–480.

[18] A.H. Barral, P. Angeli, Investigation of stratified, horizontal oil–water flow via statistical analysis of conductance probe data, Exp. Fluids 54 (10) (2013) 1604.

[19] A.D.D. Craik, The origins of water wave theory, Annu. Rev. Fluid Mech. 36 (2004) 1–28.

[20] P.G. Drazin, W.H. Reid, Hydrodynamic Stability, Cambridge University Press, 2004.

[21] T. Al-Wahaibi, P. Angeli, Transition between stratified and non-stratified horizontal oil–water flows. Part I: stability analysis, Chem. Eng. Sci. 62 (2007) 2915–2928.

[22] T. Al-Wahaibi, P. Angeli, Transition between stratified and non-stratified horizontal oil–water flows. Part II: mechanism of drop formation, Chem. Eng. Sci. 62 (2007) 2929–2940.

[23] G.B. Wallis, One-Dimensional Two-Phase Flow, McGraw Hill, 1969.